remote sensing

MDPI

Article

Quantifying the Artificial Reduction of Glacial Ice Melt in a Mountain Glacier (Urumqi Glacier No. 1, Tien Shan, China)

Shuangshuang Liu [1,2], Feiteng Wang [1,*], Yida Xie [1,2], Chunhai Xu [1], Yuang Xue [1,2], Xiaoying Yue [1] and Lin Wang [1]

[1] State Key Laboratory of Cryospheric Science, Northwest Institute of Eco-Environment and Resources, Chinese Academy of Sciences, Lanzhou 730000, China; liushuangshuang@nieer.ac.cn (S.L.); ydxie@lzb.ac.cn (Y.X.); xuchunhai@lzb.ac.cn (C.X.); xueyuang@lzb.ac.cn (Y.X.); yuexiaoying@lzb.ac.cn (X.Y.); wanglin@lzb.ac.cn (L.W.)

[2] University of Chinese Academy of Sciences, Beijing 100049, China

* Correspondence: wangfeiteng@lzb.ac.cn

Abstract: Artificial glacier melt reduction is gaining increasing attention because of rapid glacier retreats and the projected acceleration of future mass losses. However, quantifying the effect of artificial melt reduction on glaciers in China has not been currently reported. Therefore, the case of Urumqi Glacier No.1 (eastern Tien Shan, China) is used to conduct a scientific evaluation of glacier cover efficiency for melt reduction between 24 June and 28 August 2021. By combining two high-resolution digital elevation models derived from terrestrial laser scanning and unmanned aerial vehicles, albedo, and meteorological data, glacier ablation mitigation under three different cover materials was assessed. The results revealed that up to 32% of mass loss was preserved in the protected areas compared with that of the unprotected areas. In contrast to the unprotected glacier surface, the nanofiber material reduced the glacier melt by up to 56%, which was significantly higher than that achieved by geotextiles (29%). This outcome could be attributed to the albedo of the materials and local climate factors. The nanofiber material showed higher albedo than the two geotextiles, dirty snow, clean ice, and dirty ice. Although clean snow had a higher albedo than the other materials, its impact on slowing glacier melt was minor due to the lower snowfall and relatively high air temperature after snowfall in the study area. This indicates that the efficiencies of nanofiber material and geotextiles can be beneficial in high-mountain areas. In general, the results of our study demonstrate that the high potential of glacier cover can help mitigate issues related to regions of higher glacier melt or lacking water resources, as well as tourist attractions.

Keywords: artificial melt reduction; terrestrial laser scanning; unmanned aerial vehicle; material; Urumqi Glacier No.1; Chinese Tien Shan; glaciology

Citation: Liu, S.; Wang, F.; Xie, Y.; Xu, C.; Xue, Y.; Yue, X.; Wang, L. Quantifying the Artificial Reduction of Glacial Ice Melt in a Mountain Glacier (Urumqi Glacier No. 1, Tien Shan, China). *Remote Sens.* **2022**, *14*, 2802. https://doi.org/10.3390/rs14122802

Academic Editors: Anshuman Bhardwaj and Lydia Sam

Received: 18 April 2022
Accepted: 9 June 2022
Published: 10 June 2022

1. Introduction

In the European Alps, glaciers are an economic factor, contributing to hydroelectric power and serving as parts of ski resorts [1]. Recently, some efforts have been undertaken to maintain snow in ski resorts [2,3] and manage meltwater production [4]. Covering glaciers with geotextiles has become widespread as an effective method to mitigate glacier ablation in Switzerland and Austria [1,5,6]. In Asia, mountain glaciers as 'water towers' are particularly important in semi-arid regions that lack sufficient precipitation water supply seasonally [7,8]. People in Central Asia rely heavily on glacier and snow melt for their water supplies [8]. Thus, international efforts to artificially reduce glacier melt are necessary in this region, given the better water storage and management of glaciers and snow.

Various materials and technologies have been developed to protect snow and ice. For example, glacier cover, artificial snow, and water injection have been applied to reduce the glacier melt rates in a few small glaciers and glacier ski resorts [1,6]. Of these

methods, glacier cover has been shown to have a significant impact on melting and is practical in Alpine ski resort operations [9,10]. For example, geotextiles have higher albedo—they reflect more incoming shortwave radiation—than a melting glacier's surface. According to previous studies, geotextiles can slow down glacier melting by approximately 50–70% compared with unmanaged areas [4–6,9,10]. These approaches have been utilized on glaciers in the European Alps. Geotextiles could be installed in accumulation or ablation areas before the ablation season. During the winter months, materials in the accumulation or ablation areas should be moved to guarantee accumulation and the material's efficiency [11].

However, so far, the quantification of the mitigation effects of glacier cover has never been carried out in China. Furthermore, in current glacier-protection studies, the quantification of the impact of artificial melt reduction is limited by point measurements of field observations and the low spatiotemporal resolution of long-range remote sensing methods [1,10]. Moreover, only artificial snowfall has been preliminarily tested in China to reduce glacier melt [12], but snow production by machines is impossible or too risky due to weather uncertainties [2]. The type of material that is most effective in reducing the rate of glacier ablation has not been systematically evaluated. Consequently, there is an urgent need to use high-resolution technologies in glaciology research to quantify the mitigation effects of different covering materials on glacier ablation in China.

In this study, we selected Urumqi Glacier No.1 (UG1) in Tien Shan as the projected glacier. UG1 is one of the reference glaciers in the world glacier monitoring service network and provides reliable long-term observation data for documenting glacier mass balance [13,14]. During the glacier ablation period in 2021, we set up the nanofiber material and two different geotextiles on the tongue of the glacier's surface. This study aimed to evaluate (i) the protective efficiency of various covering materials on UG1 based on terrestrial laser scanning (TLS) and unmanned aerial vehicle (UAV) surveys; (ii) the possible reasons for differences in glacier ablation mitigation with different covering materials by combining albedo, mass balance, and meteorological data; and (iii) the feasibility of the artificial reduction of glacier melt for continental glaciers.

2. Study Site

UG1 (43°07′30″ N, 86°49′30″ E) is a northeast-oriented valley glacier with an area of 1555 km^2, as recorded in 2015, located on the northern slope of the Tianger Summit II (4848 m above sea level (a.s.l.)) in eastern Tien Shan (Figure 1). It is composed of eastern and western branches. Its elevation ranges from 3743 to 4484 m a.s.l. The Tien Shan Glaciological Station has conducted intensive glaciological observations of UG1 since 1959. From 1980 to 2008, the glacier experienced two accelerated mass losses that commenced in 1985 and 1996 [13]. The average annual equilibrium line altitude (ELA) was 4080 m a.s.l., and the glacier's ELA showed an upward trend during the period of 1959–2021. From 1980 to 2021, the ELA of the east branch and the west branch increased by 193 m and 282 m, respectively. The ELA of Urumqi Glacier No.1 was 4275 m a.s.l. (4200 m a.s.l. for the eastern branch and 4350 m a.s.l. for the western branch) in 2021 [15] (Figure 1b).

UG1 is a typical summer-accumulation-type glacier with a continental climate [13,14]. Precipitation mainly originates from water vapor transported by westerlies [16]. Approximately 78% of the total annual precipitation occurs from May to August (summer), dominated by solid precipitation [17]. During the winter months, the area is affected by the Siberian anticyclonic circulation [18], producing low air temperature and little precipitation. These climatic situations were recorded by the Daxigou Meteorological Station (3539 m a.s.l.), situated approximately 3 km southeast of UG1. The annual mean air temperature is −4.9 °C, and the mean yearly precipitation is 469 mm. The climatic conditions determine that both strong ablation and accumulation of UG1 mainly occur from May to August; accumulation is weak during the other months.

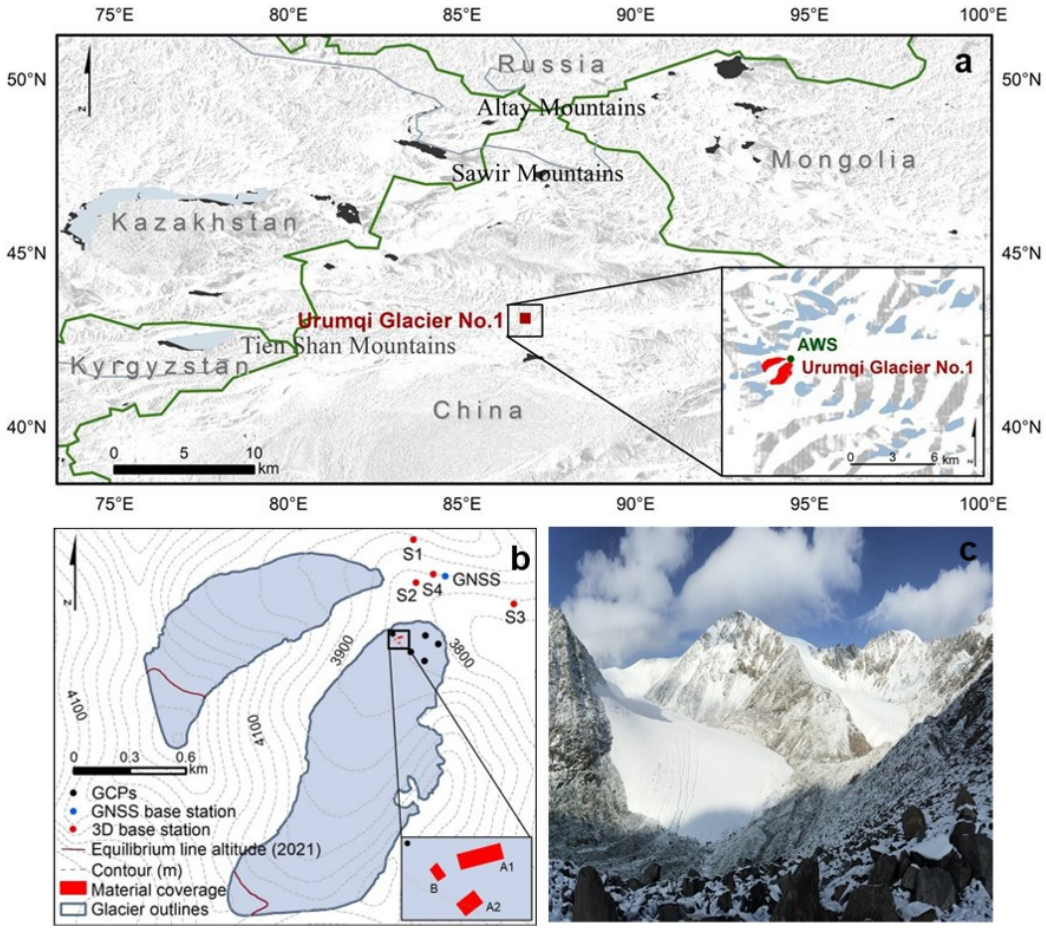

Figure 1. (**a**) Location of UG1 and Tien Shan. (**b**) The extent of the monitored area with artificial melt reduction in UG1. (**c**) Overview of the glacier tongue.

3. Data and Methodology

3.1. Artificial Glacier Melt Reduction Experiment

To slow down glacier retreat, a preliminary trial was carried out at the tongue of UG1. We installed nanofiber material and two types of geotextiles at elevations between 3800 and 3900 m a.s.l. (Figure 1). The experimental period was from 24 June to 28 August 2021. At the time of installation, the nanofiber material and geotextiles had areas of 100 and 350 m^2, respectively (Figure 2). The geotextiles were divided into two parts with areas of 200 m^2 and 150 m^2. We drilled stakes next to the covered material area for mass-balance observations (see Section 3.2). To map the extent of areas covered with materials, we relied on high-resolution imagery acquired by the TLS and UAV surveys (see Section 3.3). The TLS survey on 24 June was conducted for the east branch of UG1, whereas the UAV survey on 28 August focused on the tongue of the east branch (3740–3830 m a.s.l). Subsequently, we used the elevation range between the two survey dates. In addition, we recorded the air temperature and precipitation during the experiment and measured the reflectivity of ice, snow, and the materials at 325–1075 nm (see Sections 3.4 and 3.5).

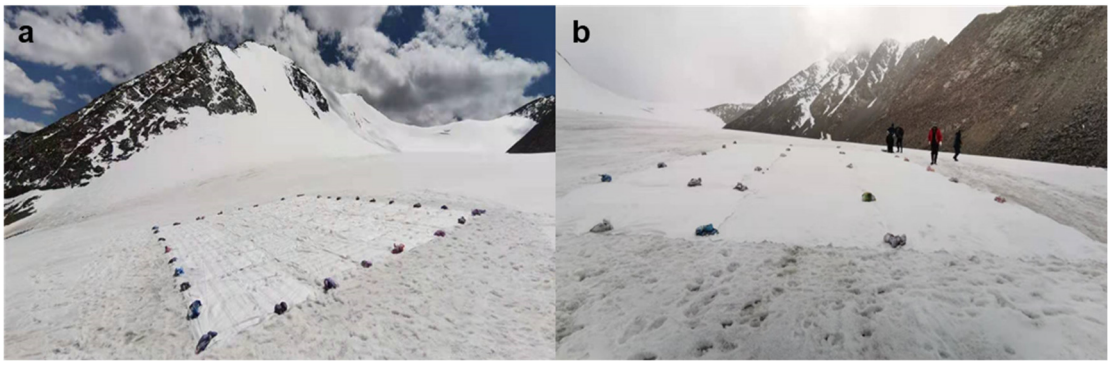

Figure 2. Covered nanofiber material (**a**) and geotextile (**b**) on 24 June 2021.

3.2. Glaciological Mass Balance

The mass balance could be calculated from the stakes or snow pits on 24 June and 28 August 2021. We drilled three new ablation stakes into the glacier's surface covered by two geotextiles and nanofiber materials in the east branch. There were five ablation stakes around the experimental site for the long-term mass balance measurement of UG1 (Figure 1b). The observations included the stake's vertical height above the glacier's surface, thickness of superimposed ice, and thickness and density of each snow/firn layer. The single-point mass balance can be expressed as [19]:

$$b_n = b_s + b_{ice} + b_{si} \quad (1)$$

where b_s, b_{ice}, and b_{si} are the mass balances of the snow, glacier ice, and superimposed ice, respectively. The uncertainty of the glaciological mass balance was ±0.2 m w.e., without considering the system's uncertainty [20].

3.3. Geodetic Mass Balance

3.3.1. TLS Digital Elevation Model (DEM)

The first survey was conducted using a Riegl VZ®-6000 (Riegl Laser Measurement Systems GmbH, Horn, Austria; 2012; weight, 14.5 kg) terrestrial laser scanner on the east branch of UG1 on 24 June 2021. TLS data for UG1 were collected from four scan positions (Figure 1b). We fixed each scanning position with reinforced concrete to obtain the precise point cloud coordinates. The real-time kinematic–global navigation satellite system (RTK-GNSS, Unistrong E650 instrument) positioning measured four scanning positions to acquire precise point cloud georeferencing. Scans were performed on a sunny day to reduce the effect of precipitation and fog. To obtain a fine scan of the glacier's surface, we first set the repetition rate of the laser pulse to 50 kHz with vertical and horizontal angle ranges of 60–120° from zenith and 0–360°, respectively. Then, the repetition rate was set to 30 kHz and the overlap percentage of four scans was at least 30% [21].

Point cloud data were processed using RiSCAN PRO® v 1.81. First, we converted these data from the scanner coordinate system to a global coordinate system using four scan positions. In the second step, we used multi-station adjustment to register the data for each scan location according to the iterative closest point algorithm [22,23]. Subsequently, point cloud data compression was conducted using an octree algorithm to generate equally spaced points for the merged layer [24]. The terrain filter was then used to filter out noise and non-terrestrial data that resulted from atmospheric reflection, such as dust or moisture [25]. Finally, the DEM with a spatial resolution of 0.5 m was generated from the TLS measurement.

3.3.2. UAV DEM

The second survey was conducted using a lightweight UAV in the ablation zone of UG1 on 28 August 2021. A Phantom 4 RTK from DJI was used. It is a fixed-wing UAV

capable of a flight time of approximately 15 min when the UAV takes off above 3800 m a.s.l. The UAV was equipped with a GNSS and a small 20-megapixel digital camera, which was electronically activated by the automatic system to obtain images at the required place. During the survey, we collected 775 images along 15 north–south routes. The selected image overlap was 80% in both the transverse and longitudinal directions of the UAV flight path. This level of redundancy ensured that there were no gaps in stereo coverage. Before the aerial survey, we used RTK-GNSS (Unistrong E650, Beijing, China) to collect five stakes on the glacier's surface as ground control points (GCPs) (Figure 1). The accuracy of this survey was ±1 cm in the horizontal direction and ±2 cm in the vertical direction [26].

The UAV-collected images and GCPs were processed with Pix4D Mapper. First, we adopted the structure from motion (SfM) to create a sparse 3D point cloud [27]. Next, multi-view stereo methods were applied to derive a higher point cloud density [28]. The use of GCPs or in combination with camera GPS positions allowed for the georeferencing of the 3D model in a coordinate system. Finally, DEM and ortho-photo mosaics were generated at a spatial resolution of 0.03 m. The DEM was resampled to a resolution of 0.5 m, and the world geodetic system 1984 (WGS84) datum (EPSG: 4326) and UTM 45N projection were used for coordinate normalization.

3.3.3. Co-Registration of DEMs and Mass Balance Calculation

Because of the different surveying techniques, horizontal and vertical distortions may exist between the TLS and UAV DEM. Therefore, two DEMs need to be registered before calculating the elevation changes [29]. Given the high resolution of the UAV DEM, some identifiable bedrocks and boulders in off-glacier regions were selected as a reference to co-register the TLS DEM. After the relative registration procedure, the geodetic mass balance was obtained based on the different DEMs.

$$B_{\text{geod}} = \frac{\Delta V}{S} \times \frac{\rho_{\text{ice}}}{\rho_{\text{water}}} \tag{2}$$

where ΔV is the total volume change, S is the glacier area, ρ_{water} is the density of water, and ρ_{ice} is the density of ice [14]. Only bare ice melted during the mass balance observation period, and no firn was found. Thus, the ice density was used conservatively in our study.

3.3.4. Uncertainty Assessment

The error in the geodetic mass balance had two primary sources: glacier elevation change ($\sigma_{\overline{\Delta h}}$) and volume-to-mass conversion (σ_ρ). Uncertainties related to the geodetic mass balance (σ_{geod}) were calculated as [30,31]:

$$\sigma^2_{\overline{\Delta h}} = \sigma^2_{\Delta h} \frac{1}{5} \frac{S_{cor}}{S} \tag{3}$$

$$\sigma_{\text{geod}} = \sqrt{\left(\overline{\Delta h}\sigma_\rho\right)^2 + \left(\rho\sigma_{\overline{\Delta h}}\right)^2} \tag{4}$$

where $\sigma_{\Delta h}$ is the standard deviation of the stable terrain, S is the glacier area, S_{cor} is the spatially correlated area equal to S [1], $\overline{\Delta h}$ is the average value of the TLS and UAV-derived elevation change, and the related uncertainty relies on the accuracy of the used DEMs. Here, the value of $\sigma_{\overline{\Delta h}}$ was ±0.13 m. To convert volume change to water equivalent (w.e.) for the entire glacier, a density of 900 kg m^{-3} with an uncertainty of ±17 kg m^{-3} (σ_ρ) was used [32].

3.4. Ice and Snow Spectral Reflectance Measurements

To evaluate the mechanisms of different covering materials to reduce ablation, we measured the reflectivity data of ice, snow, two geotextiles, and nanofiber material at 325–1075 nm with an Analytical Spectral Device Field Spec Handheld 2 spectroradiometer. It had a resolution of 3 nm and an error of <4%. The measurement sensor was installed on a tripod 0.5 m above the ground, and had 25 fields of view at a point with a diameter of 0.225 m. We recalibrated our instrument under different sky radiation conditions. Measurements were taken at the direction perpendicular to the glacier surface between 12:00 and 16:00 local time (4:00–8:00 GMT). After completing the measurement, we processed the raw data from the device using spectrum analysis. Broadband albedo was calculated from the weighted mean of the spectral reflectivity and incident solar radiation over the entire spectral wavelength of each location [17,33].

3.5. Meteorological Measurements

We installed a monitoring tower near 200 m of the tongue of UG1 (Figure 1a). The monitoring tower was equipped with a high-resolution temperature sensor (PT100 RTD, ±0.1 K) 2 m above the surface. Its temperature readings could be regarded as the same as the air temperatures at the UR1 due to its proximity. We recorded the mean values for this parameter at 20 min intervals. Precipitation was measured using an automatic weighing scale (T-200B; Geonor, Branchville, NJ, USA) with an accuracy of approximately 0.1%. All sensors could operate at low temperatures (down to −55 °C).

4. Results

4.1. Effects of Glacier Ablation Mitigation

The difference in the high-resolution DEMs at the tongue of UG1 demonstrated the significant efficiency of the materials for ice ablation (Figure 3). Between 24 June and 28 August, the average elevation change, excluding that of the material-covered areas, was −2.47 m, whereas the protected area only exhibited an elevation change of 1.69 m. As a result, 32% of the glacier ablation was reduced by the materials. A1 and A2 were the geotextile-covered areas, and the average surface elevation changes were −1.81 m and −1.71 m over A1 and A2, respectively. B was the nanofiber-covered area, and its elevation change was −1.08 m. The nanofiber material reduced the melting process by 56% compared with the two geotextiles (29%). According to the density of 900 ± 17 kg m^{-3} [32], 0.70 ± 0.01 m w.e. of the total mass loss was mitigated for the protected areas. In the nanofiber material and geotextile-covered areas, the mitigation effect could reach up to 1.25 ± 0.02 m w.e. and 0.64 ± 0.01 m w.e., respectively.

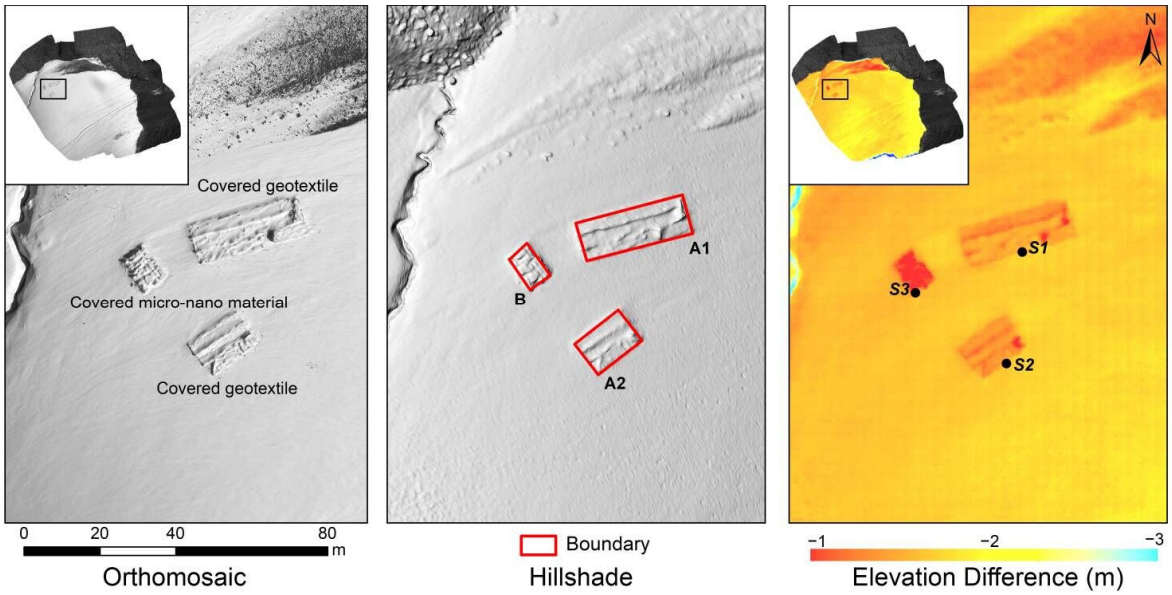

Figure 3. Ortho-mosaic on 28 August 2021 (**left** panel), hillshade generated from the DEM on 28 August 2021 (**middle** panel), and changes in elevation between 24 June and 28 August 2021 (**right** panel). Glacier ablation was monitored using ablation stakes (S1–S3).

Based on four field surveys, we used stakes to evaluate the efficiency of the nanofiber material during the study period (Figure 4). At the time of installation, the glacier surface was relatively flat. After seven days (1 July), the effect of the nanofiber material was already obvious, as the protected area was 0.18 ± 0.2 m w.e. higher than the surrounding surfaces (Figure 4a). The ice height saved by the nanofiber ranged between 0.45 ± 0.2 and 0.65 ± 0.2 m w.e. (on 9 July and 25 July, respectively) (Figure 4b,c). The last observation was carried out on 15 August, and the mean elevation change between the protected and unprotected surface was 1.26 ± 0.2 m w.e. (Figure 4d).

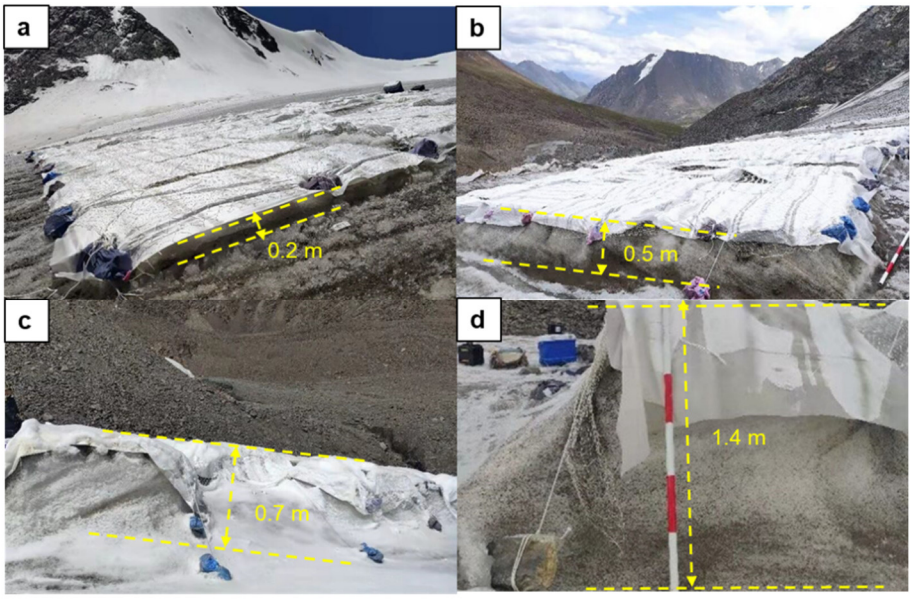

Figure 4. Effectiveness of the nanofiber material on UG1: 1 July (**a**), 9 July (**b**), 25 July (**c**), and 15 August (**d**).

4.2. Difference between the Three Covering Materials for Reducing Ablation

Figure 5 and Table 1 illustrate the significant spatial variation in the efficiency of the materials for melt reduction. In all profiles, the mass balance management thickness loss ranged between 1.05 and 1.95 m, whereas the reference area loss was between 2.12 and 2.30 m. The changes calculated during the study period were larger than the measurement errors. The difference in elevation change between the covered and uncovered areas was 0.65 m on average during the experiment period, which demonstrated the considerable effect of nanofiber coverage on ice loss. A1 and A2 saved an ice height of up to 0.35 m and 0.47 m, respectively; in contrast, B saved up to 1.14 m (Table 1).

In the longitudinal transect, the highest DEM differences between managed profiles and reference profiles were in the following order: B, A2, and A1 (Figure 5 and Table 1). A1 and A2 showed lower elevation changes than B in the mass-balance-managed profiles, although some oscillations occurred. Changes in surface elevation between the mass-balance-managed profiles and reference profiles could also be observed in the transversal transect (Figure 5 and Table 1), in which lower changes in B and higher differences between A1 and A2 were present in the covered profiles.

Figure 5 also shows small-scale effects. The area encircled by a solid black ellipse showed substantially higher efficiency owing to the double geotextile layer at the seams of the two rolls. The seams of A1 and A2 saved mass loss of up to 0.72 m and 0.64 m, respectively. However, this caused an undulation aligned in the direction of the seams. This situation amplified over time, ultimately leading to low mitigation effect and the need to replace the materials [11].

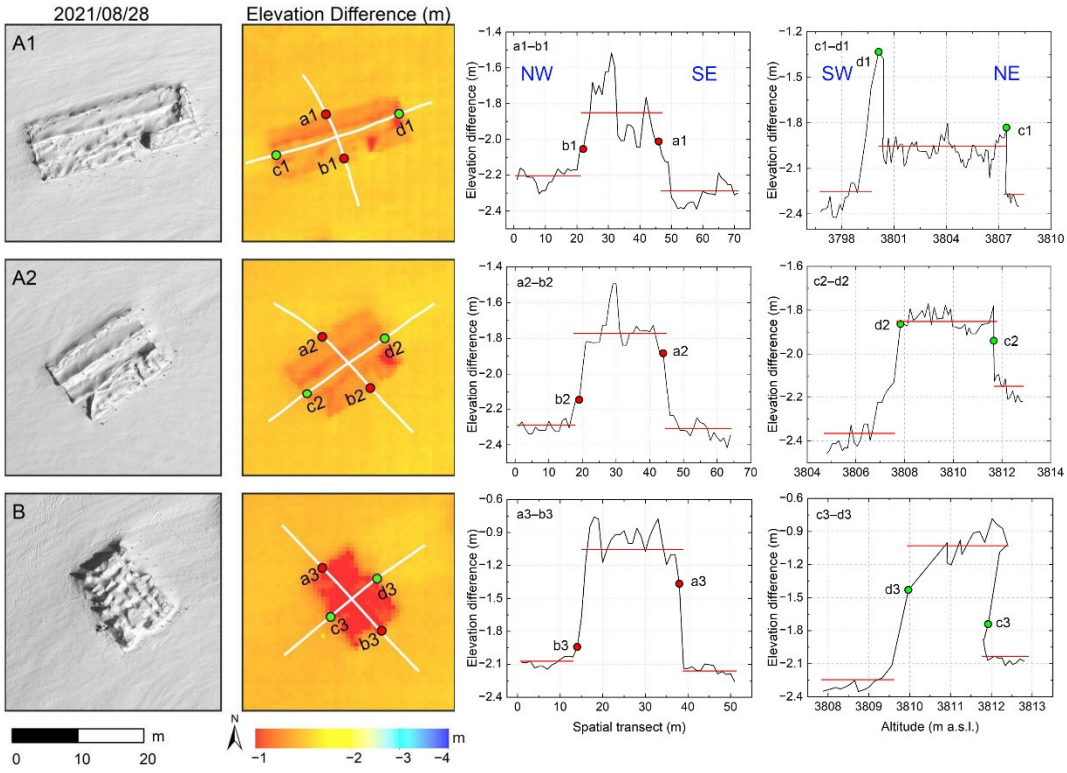

Figure 5. Detailed change in the selected area of UG1. Ortho-mosaic on 28 August 2021 (**left** panel), elevation changes between 24 June and 28 August 2021 (**middle** panel), and spatial transect differences for elevation change (**right** panel). A1 and A2 were the geotextile−covered areas. B was the nanofiber−covered area.

Table 1. Mean elevation of the profiles. The mean (μ) and standard deviation (σ) of glacier elevation changes as well as absolute differences (abs. diff) of the experimental area (exp) values to the reference area (ref) values are listed.

Profile Name	Mean Elevation (m a.s.l.)	From 24 June to 28 August				
		Ref		Exp		Abs.
		μ (m)	σ (m)	μ (m)	σ (m)	diff (m)
a1b1	3804	−2.25	0.08	−1.86	0.16	0.39
a2b2	3809	−2.30	0.06	−1.78	0.13	0.52
a3b3	3811	−2.12	0.05	−1.05	0.27	1.16
c1d1	3803	−2.26	0.17	−1.95	0.14	0.31
c2d2	3809	−2.27	0.13	−1.85	0.04	0.42
c3d3	3811	−2.17	0.15	−1.06	0.23	1.11

5. Discussion

5.1. Quality of Point Cloud Data and DEM Differencing

For TLS, the fixed scanning locations used in our fieldwork were situated at different elevations and directions relative to the glacier surface, which improved the stability of the TLS survey. The overlap percentage of point clouds was >30%, which met the requirements of data registration (CH/Z 3017-2015, 2015). Dry, windless weather conditions were selected to reduce the influence of atmospheric refraction. However, the TLS and glacier surface may have caused the acquired point cloud errors. Manufacturers generally provide simplified and constant values for precision because of unquantifiable systematic errors. A TLS precision of approximately 10 mm satisfies the measurement accuracy in glaciology [25]. This study selected the best measurement data at the ablation area to ensure good TLS DEM quality.

The point density and distribution of GCPs for UAV surveys are crucial for DEM derivation [34–36]. In our study, UAV photogrammetry was well-depicted in vertical photos owing to the homogeneity of the point density (Figures 3 and 5). All GCPs were measured with RTK-GPS to provide accurate direct geo-referencing and registration. The root-mean-square errors for the GCPs were within 0.5 m for the horizontal and vertical directions. The error sources may include the suboptimal distribution and density of the GCPs. Well-distributed GCPs could improve the accuracy of DEM, but it was difficult to access the steep slopes on either side of the glacier and deploy the GCPs. For the desired distribution, the GCPs should be evenly distributed over the glacier lateral moraines.

Additionally, systematic shifts in DEMs in the horizontal and vertical directions introduce other errors [29]. Therefore, the elevation difference in the off-glacier terrain between the TLS DEM and UAV DEM was calculated to quantify the accuracy of the results for the vertical direction. The mean vertical difference between the two DEMs was 0.02 m and had a standard deviation of 0.28 m (Figure 6); such a decimeter-scale uncertainty indicates that the DEMs used in the following analyses were aligned accurately in the vertical direction.

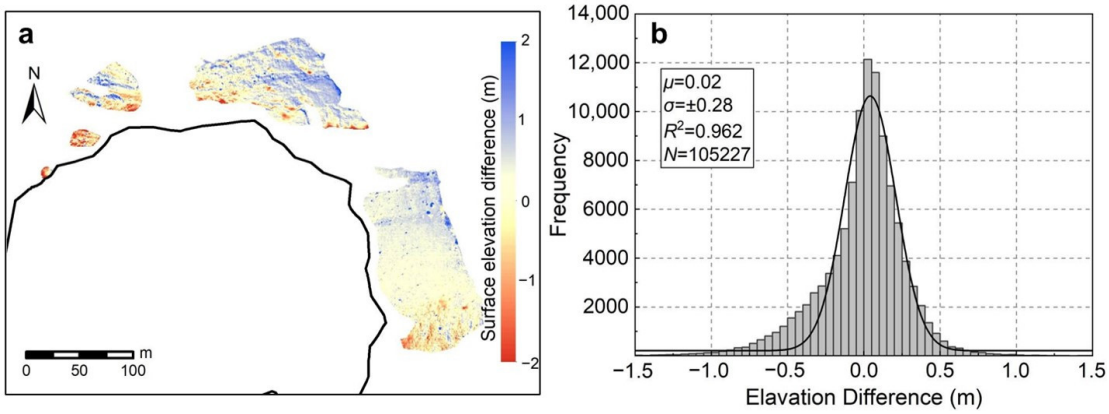

Figure 6. Spatial distribution of glacier elevation changes over stable off-glacier areas (**a**) and frequency distributions (**b**). The mean (μ), standard deviation (σ), fitting coefficient (R^2), and number of pixels (N) are listed.

5.2. Accuracy of Geodetic Surface Change

The stake observations were used to objectively evaluate the precision of the glacier elevation changes in material-covered areas. Figure 7 shows a scatter plot of the observed change in stake height versus the elevation change from the two surveys at the corresponding location. The correlation coefficient (R^2) between glaciological elevation changes and geodetic elevation changes at the same positions was 0.93, indicating that the geodetic surveys generally provided a high-accuracy elevation change. A comparison of the stake measurement and geodetic approach results produced a mean difference of 0.07 m and a relative error of 3%. These results indicate a satisfactory comparison of the geodetic and glaciological surface elevation changes.

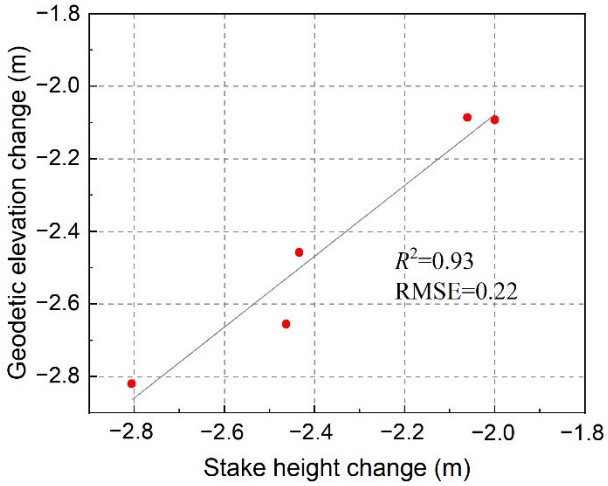

Figure 7. Comparison of the surface elevation change from two surveys and in situ measurements at each stake in the study area. The red dots represent the glaciological elevation change against geodetic elevation change at corresponding ablation stakes.

5.3. Possible Reasons for Reducing Ablation Differences

The glacier melt reduction differences between nanofiber and the two types of geotextiles may be attributed to the factors regulating the local energy balance, such as the optical and thermal properties of the materials, local climatic conditions, or topographic effects. The albedo is known to decrease with time due to the deposition of fine particulates (dust), regardless of the type of geotextile [37,38]. Thus, considering the last measurement (28 August 2021), material coverage albedo was in the following order (from higher to lower albedo): nanofiber material, geotextile with an area of 150 m^2, and

geotextile with an area of 200 m² (Figure 8). A similar comparative experiment at the Presena Ovest Glacier discussed the optical properties of geotextiles [10]. Their findings are consistent with those of our study, which showed that materials with higher albedo were the best at slowing glacier melt. However, all of the materials showed a lower albedo than that of clean snow (Figure 8); therefore, the application of materials installed on the glacier surface was conducted in the absence of seasonal snowfall. In addition, we measured the spectrally resolved reflectance of the surrounding unprotected snow and ice surfaces with different impurity coverage (Figures 8 and 9). In contrast to the geotextiles, the nanofiber material had a higher albedo than the surrounding dirty snow, clean ice, and dirty ice, which indicated the notable effectiveness of nanofiber materials in reflecting solar radiation and reducing the absorbed energy.

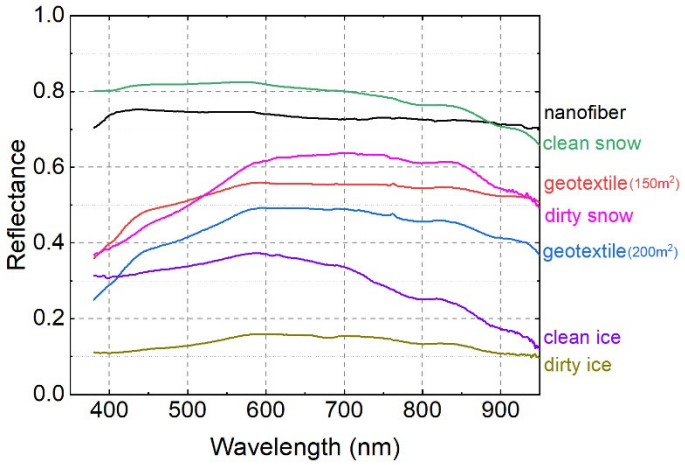

Figure 8. Spectral reflectance of materials and surrounding snow and ice surfaces. The situations of the observation surface are shown in Figure 9.

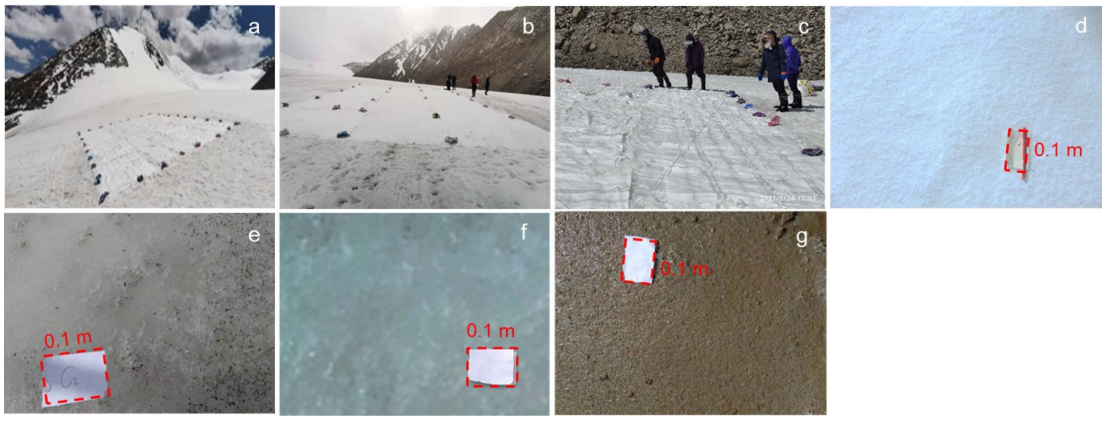

Figure 9. Images of the surface of UG1 and measured albedo (α) values. (**a**–**g**) represent the nanofiber material, geotextile with an area of 150 m², geotextile with an area of 200 m², clean snow, dirty snow, clean ice, and dirty ice, respectively.

As shown in Figure 8, the albedo of clean snow was higher than that of the geotextiles and nanofiber material. Once snowfall occurs, it rapidly whitens the glacier's surface and increases its albedo. We presumed that solid precipitation also played a significant role in slowing glacier ablation during the experiment. We applied a sinusoidal function to identify the amount of solid precipitation accumulated on the glacier surface [39]. This function gives the conversion between liquid and solid precipitation in the temperature range of +2 to +4 °C [40,41]. When the air temperature is below 2 °C, solid precipitation (snow) occurs, and between 2 and 4 °C, rainfall with snow occurs. In our study, the mean air temperature was approximately 5 °C and the total precipitation was 231 mm. Only a 12-

day snowfall event occurred, but there was no continuous solid precipitation for a week (Figure 10). During 16–19 August 2021, there was solid precipitation for four consecutive days, with a total snowfall of 41 mm. However, effective snowfall accumulation in the ablation area is difficult because of the relatively high air temperature after snowfall. Based on the 1988–1989 stake data, the mass balance of UG1 below 3900 m a.s.l. was negative in the summer, indicating that the glacier's surface experienced ablation [42]. Our stake observation results also showed negative mass balance values (Figure 7). Therefore, in the study area controlled by high air temperature, solid precipitation during the experiment period had a minor impact on slowing glacier melt compared with the geotextiles and nanofiber material. In contrast, the prepared nanofiber material exhibited excellent cooling performance owing to selective thermal emissions. An outdoor experiment demonstrated that the material exhibited a sub-ambient temperature drop of 5 °C, even at a peak solar intensity of approximately 900 W m^{-2} in the daytime, and ~7 °C below the ambient temperature at night, excluding the effect of sunlight [43]. For future practical applications, durability is a crucial property for radiative-cooled materials.

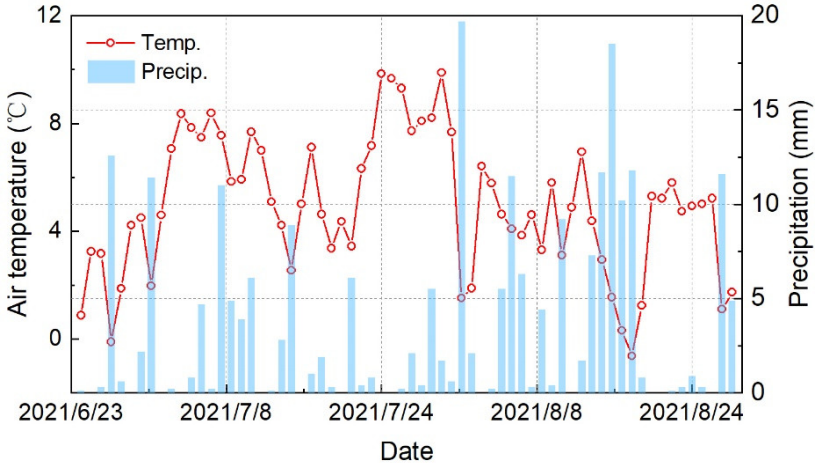

Figure 10. Air temperature and precipitation measured at the automatic weather station from 24 June to 28 August 2021.

In addition to the material properties, the effect of artificial glacier melt reduction may depend on topographical parameters, such as the slope, aspect, and elevation of the site [11]. These factors influence the relative importance of the energy balance components altered by material coverage. For example, this theoretically means that the sites with the greatest input of solar radiation were more efficient because the materials efficiently reduced shortwave radiation [6]. However, the number of available studies that have investigated or included these dependencies is fewer. Our study did not account for such topographical parameters, but these dependencies should be further researched.

5.4. Compared with Previous Similar Studies

Previous experiments on artificial measures to slow down glacier melt were performed in the European Alps (Table 2). These geotextiles could reduce glacier melting by 50–70% compared with the uncovered glacier surface. However, using geotextiles on UG1 was less efficient than similar experiments conducted in Europe. This difference may be related to factors that alter the local energy balance, such as albedo changes, local climatic conditions, and topographical influences [10]. However, the number of available studies (Table 2) to investigate or include these dependencies is too small, and our consideration was based on the mean of ε_0 (ε_0 refers to the percentage reduction in melting compared with an uncovered location). Moreover, using nanofibers on UG1 had a significant effect, which could slow down the ablation of the glacier by 56%. The different material properties of covers are key parameters affecting their performance in reducing snow and ice

ablation [9]. These properties directly or indirectly affect the energy balance of snow and ice surfaces in different ways. Therefore, further efforts will consider a basic comparison of the different mass and energy balance regimes, comparing the basic settings of UG1 to other studies.

Table 2. Studies documenting local melt reduction by geotextiles. ϵ_0 refers to the percentage reduction in melting compared with an uncovered location.

Glacier (Country)	Tested Period	Latitude (N)	Longitude (E)	Altitude (m a.s.l.)	Area (m^2)	Material's Chemical Composition	ϵ_0 (%)	Source
Dosdè Est (Italy)	15 May 2008–4 October 2008	46°23′	10°13′	2800	150	Polyester, polypropylene	69	[10]
Presena Ovest (Italy)	28 June 2010–14 September 2010	46°13′	10°34′	2765	600	Polypropylene	49	[10]
Schaufelferner (Austria)	22 June 2005–16 September 2005	46°59′	11°07′	2870	180	Polyester, polypropylene	60	[9]
Mount Aragatz (Armenia)	29 June 2012–22 June 2013	40°28′	44°10′	3200	20,000	Double-bedded polypropylene/polyester	57	[4]
UG1 (China)	24 June 2021–28 August 2021	43°07′	86°49′	3800	350	Polypropylene	29	This study
UG1 (China)	24 June 2021–28 August 2021	43°07′	86°49′	3800	100	Cellulose acetate molecules	56	This study

5.5. Feasibility Analysis of the Artificial Reduction of Glacier Melt

Based on the positive results for UG1, glacier covers can be applied to natural glaciers. Previously, there have been benefits of such measures at a local scale. In Switzerland, glaciers have been actively covered with geotextiles for 15 years to reduce the accelerated ice melting caused by atmospheric warming. This technology mitigates approximately 350,000 m^3 of ice melt annually [11]. Seasonal water shortages in arid areas affect irrigation and the domestic water supply. Therefore, seasonal reservoirs have been established through the artificial management of snow and ice melt [44,45]. Geotextiles placed over a glacier's surface can delay peak meltwater by 1–2 months into dry summers [4]. This provides a valuable way to store water for local agriculture in arid regions. In the Austrian Alps, geotextiles installed in glacier ski resorts can reduce the negative effects of glacier retreat on ski resort infrastructure [10,46]. Thus, the present artificial glacier melt reduction on a local scale provides an effective method for areas with rapid glacier melting and a lack of water resources or in other tourist attraction areas.

Although the above analysis showed that such measures were beneficial at a local scale, the recovery operations of the materials were difficult. Geotextiles often broke and were replaced with new ones because of their cold and frozen surfaces, thus increasing the cost. Geotextiles are composed of polypropylene fibers. Geotextile degradation may also negatively affect the local environment and the downstream water quality. Nanofibers typically consist of abundant and eco-friendly cellulose acetate molecules. They are biodegradable and can be digested by microorganisms in nature [47]. Thus, further studies are needed to assess the effective glacier volume saved by artificial melt reduction, the financial cost of saving glacier ice, and the environmental sustainability if larger areas (such as all ablation zones of a glacier) are to be covered.

Note that artificial melt reduction measures were determined only in the ablation area of UG1 in this study. For glacier ski resorts in Austria, this approach has the potential to maintain the surface stability at the accumulation areas of the glaciers, thus preserving the glacier's resources [1]. However, UG1 is a summer-accumulation-type glacier, and 78% of the total annual precipitation (mainly solid) occurs from May to August [17]. While ablation also occurred in the accumulation areas in the summer, the amount of ablation was smaller [48]. This situation may limit the effect of glacier ablation mitigation, as

covering materials can easily prevent snow accumulation. Thus, mass balance management at glacier tongues is feasible in situations where the managed area does not need to be extended to the accumulation areas of the glaciers.

In addition to the glacier cover approach, the application of artificial precipitation activities to glaciers is a promising option, which is known to target the amplification of accumulation. The albedo of snow was higher than that of ice, thus achieving more significant glacier retreat mitigation. Technical snow production on glaciers has less impact on the downstream environment and is a more realistic view of a protected glacier [11]. The efficiency of this method and that of geotextile coverage can be combined in the future to effectively preserve glacier melting.

6. Conclusions

This study takes UG1 in the Tien Shan Mts. as an example and provides the first estimate of the mitigation effect of different covering materials on glacier melt reduction between 24 June and 28 August 2021. By surveying the glacier surface elevation changes between TLS and UAV, an efficiency of 32% in melt reduction was found beneath the installed materials compared with that of the uncovered surfaces. During this period, the efficiency of the installed nanofiber to reduce snow and ice melt was 56%, approximately 27% higher than that of the two types of geotextiles. The average difference in thickness loss between the protected and unprotected areas was 1.14 m for nanofiber and 0.41 m for the two geotextiles in all profiles, demonstrating the considerable effect of nanofiber coverage on ice loss.

Field information regarding the surface albedo of the materials and the local climatic conditions was collected for UG1, allowing the determination of the possible factors affecting ablation differences. We found that the nanofiber material had a higher albedo than the two types of geotextiles and surrounding dirty snow, clean ice, and dirty ice, which suggested a strong effectiveness of the nanofiber material in reflecting solar radiation and in decreasing the absorbed energy. Although clean snow had a higher albedo than the other materials, its impact on slowing glacier melt in the ablation area of the glacier was minor in dry climates.

Our study demonstrated that the effect of materials on glacier melt reduction is significant. This approach can be widely promoted in areas with rapid glacier melting and a lack of water resources, or in other tourist attraction areas. Our current work is a preliminary experiment. Further efforts will consider the effective glacier volume saved by artificial melt reduction, the financial cost of saving glacier ice, and the environmental sustainability if larger areas were to be covered. Nevertheless, using geotextiles on UG1 was less efficient than similar experiments conducted in Europe. Further efforts will consider a basic comparison of the different mass and energy balance regimes comparing the basic settings of UG1 with other studies. The technical production of snow on glaciers is also a promising alternative. A combination of artificial snowfall and glacier cover could be a good option to reduce the melting of glaciers in the future.

Author Contributions: Conceptualization, S.L. and F.W.; methodology, S.L.; software, Y.X. (Yuang Xue); validation, S.L., F.W. and Y.X. (Yida Xie); formal analysis, S.L. and C.X.; investigation, Y.X. (Yida Xie); resources, L.W.; data curation, X.Y.; writing—original draft preparation, S.L.; writing—review and editing, S.L. and F.W.; visualization, S.L.; supervision, F.W.; project administration, S.L.; funding acquisition, F.W. All authors have read and agreed to the published version of the manuscript.

Funding: This research was funded by the State Key Laboratory of Cryospheric Science (SKLCS-ZZ-2022), the National Key R&D Program of China (2020YFF0304400), the National Natural Science Foundation (41721091 and 42001067), and Natural Science Foundation of Gansu Province (21JR7RA059).

Data Availability Statement: The reflectivity data of ice and snow related this study were published by Yue et al. (2017). The equilibrium line altitude data were submitted to the WGMS and are

available at the following website: http://dx.doi.org/10.5904/wgms-fog-2021-05 (accessed on 28 May 2022) (WGMS, 2021). TLS and UAV point cloud data are available upon request by email to the corresponding author.

Conflicts of Interest: The authors declare no conflict of interest.

References

1. Fischer, A.; Helfricht, K.; Stocker-Waldhuber, M. Local reduction of decadal glacier thickness loss through mass balance management in ski resorts. *Cryosphere* **2016**, *10*, 2941–2952. https://doi.org/10.5194/tc-10-2941-2016.
2. Gruenewald, T.; Wolfsperger, F.; Lehning, M. Snow farming: Conserving snow over the summer season. *Cryosphere* **2018**, *12*, 385–400. https://doi.org/10.5194/tc-12-385-2018.
3. Spandre, P.; Morin, S.; Lafaysse, M.; Lejeune, Y.; Francois, H.; George-Marcelpoil, E. Integration of snow management processes into a detailed snowpack model. *Cold Reg. Sci. Technol.* **2016**, *125*, 48–64. https://doi.org/10.1016/j.coldregions.2016.01.002.
4. Nestler, A.; Huss, M.; Ambartzumian, R.; Hambarian, A.J.G. Hydrological Implications of Covering Wind-Blown Snow Accumulations with Geotextiles on Mount Aragats, Armenia. *Geosciences* **2014**, *4*, 73–92. https://doi.org/10.3390/geosciences4030073.
5. Olefs, M.; Obleitner, F. Numerical simulations on artificial reduction of snow and ice ablation. *Water Resour. Res.* **2007**, *43*, 71–81. https://doi.org/10.1029/2006wr005065.
6. Olefs, M.; Lehning, M. Textile protection of snow and ice: Measured and simulated effects on the energy and mass balance. *Cold Reg. Sci. Technol.* **2010**, *62*, 126–141. https://doi.org/10.1016/j.coldregions.2010.03.011.
7. Immerzeel, W.W.; Lutz, A.F.; Andrade, M.; Bahl, A.; Baillie, J.J.N. Importance and vulnerability of the world's water towers. *Nature* **2020**, *577*, 364–369. https://doi.org/10.1038/s41586-019-1822-y.
8. Farinotti, D.; Longuevergne, L.; Moholdt, G.; Duethmann, D.; MoLg, T.; Bolch, T.; Vorogushyn, S. Substantial glacier mass loss in the Tien Shan over the past 50 years. *Geoscience* **2015**, *8*, 716–722. https://doi.org/10.1038/NGEO2513.
9. Olefs, M.; Fischer, A. Comparative study of technical measures to reduce snow and ice ablation in Alpine glacier ski resorts. *Cold Reg. Sci. Technol.* **2008**, *52*, 371–384. https://doi.org/10.1016/j.coldregions.2007.04.021.
10. Senese, A.; Azzoni, R.S.; Maragno, D.; D'Agata, C.; Fugazza, D.; Mosconi, B.; Trenti, A.; Meraldi, E.; Smiraglia, C.; Diolaiuti, G. The non-woven geotextiles as strategies for mitigating the impacts of climate change on glaciers. *Cold Reg. Sci. Technol.* **2020**, *173*, 103007. https://doi.org/10.1016/j.coldregions.2020.103007.
11. Huss, M.; Schwyn, U.; Bauder, A.; Farinotti, D. Quantifying the overall effect of artificial glacier melt reduction in Switzerland, 2005–2019. *Cold Reg. Sci. Technol.* **2021**, *184*, 103237. https://doi.org/10.1016/j.coldregions.2021.103237.
12. Wang, F.; Yue, X.; Wang, L.; Li, H.; Du, Z.; Ming, J.; Li, Z. Applying artificial snowfall to reduce the melting of the Muz Taw Glacier, Sawir Mountains. *Cryosphere* **2020**, *14*, 2597–2606. https://doi.org/10.5194/tc-14-2597-2020.
13. Li, Z.; Li, H.; Chen, Y. Mechanisms and Simulation of Accelerated Shrinkage of Continental Glaciers: A Case Study of Urumqi Glacier No. 1 in Eastern Tianshan, Central Asia. *J. Earth. Sci.* **2011**, *22*, 423–430. https://doi.org/10.1007/s12583-011-0194-5.
14. Zemp, M.; Thibert, E.; Huss, M.; Stumm, D.; Denby, C.R.; Nuth, C.; Nussbaumer, S.U.; Moholdt, G.; Mercer, A.; Mayer, C.; et al. Reanalysing glacier mass balance measurement series. *Cryosphere* **2013**, *7*, 1227–1245. https://doi.org/10.5194/tc-7-1227-2013.
15. World Glacier Monitoring Service (WGMS). *Fluctuations of Glaciers Database*; World Glacier Monitoring Service: Zurich, Switzerland, 2013. https://doi.org/10.5904/wgms-fog-2021-05.
16. Han, T.; Ding, Y.; Ye, B.; Liu, S.; Jiao, K. Mass-balance characteristics of Urumqi glacier no. 1, Tien Shan, China. *Ann. Glaciol.* **2006**, *43*, 323–328. https://doi.org/10.3189/172756406781811961.
17. Yue, X.; Zhao, J.; Li, Z.; Zhang, M.; Fan, J.; Wang, L.; Wang, P. Spatial and temporal variations of the surface albedo and other factors influencing Urumqi Glacier No. 1 in Tien Shan, China. *J. Glaciol.* **2017**, *63*, 899–911. https://doi.org/10.1017/jog.2017.57.
18. Moelg, T.; Maussion, F.; Scherer, D. Mid-latitude westerlies as a driver of glacier variability in monsoonal High Asia. *Nat. Clim. Change* **2014**, *4*, 68–73. https://doi.org/10.1038/nclimate2055.
19. Wang, P.; Li, Z.; Li, H.; Wang, W.; Zhou, P.; Wang, L. Characteristics of a partially debris-covered glacier and its response to atmospheric warming in Mt. Tomor, Tien Shan, China. *Glob. Planet. Chang.* **2017**, *159*, 11–24. https://doi.org/10.1016/j.gloplacha.2017.10.006.
20. Zemp, M.; Jansson, P.; Holmlund, P.; Gartner-Roer, I.; Koblet, T.; Thee, P.; Haeberli, W. Reanalysis of multi-temporal aerial images of Storglaciaren, Sweden (1959–99)—Part 2: Comparison of glaciological and volumetric mass balances. *Cryosphere* **2010**, *4*, 345–357. https://doi.org/10.5194/tc-4-345-2010.
21. Mukupa, W.; Roberts, G.W.; Hancock, C.M.; Al-Manasir, K. A review of the use of terrestrial laser scanning application for change detection and deformation monitoring of structures. *Surv. Rev.* **2017**, *49*, 99–116. https://doi.org/10.1080/00396265.2015.1133039.
22. Besl, P.J.; McKay, N.D. A method for registration of 3-d shapes. In *Sensor Fusion IV: Control Paradigms and Data Structures*; SPIE: Philadelphia, PA, USA, 1992; Volume 1611, pp. 586–606. https://doi.org/10.1117/12.57955.
23. Zhang, Z.Y. Iterative point matching for registration of free-form curves and surfaces. *Int. J. Comput. Vis.* **1994**, *13*, 119–152. https://doi.org/10.1007/bf01427149.
24. Perroy, R.L.; Bookhagen, B.; Asner, G.P.; Chadwick, O.A. Comparison of gully erosion estimates using airborne and ground-based LiDAR on Santa Cruz Island, California. *Geomo* **2010**, *118*, 288–300. https://doi.org/10.1016/j.geomorph.2010.01.009.

25. RIEGL Laser Measurement Systems. *3D Terrestrial Laser Scanner Riegl VZ®-4000/Riegl VZ®-6000 General Description and Data Interfaces*; RIEGL Laser Measurement Systems: Horn, Austria, 2014; pp. 1–466.
26. Xu, C.; Li, Z.; Wang, F.; Li, H.; Wang, W.; Wang, L. Using an ultra-long-range terrestrial laser scanner to monitor the net mass balance of Urumqi Glacier No. 1, eastern Tien Shan, China, at the monthly scale. *J. Glaciol.* **2017**, *63*, 792–802. https://doi.org/10.1017/jog.2017.45.
27. Turner, D.; Lucieer, A.; Watson, C. An Automated Technique for Generating Georectified Mosaics from Ultra-High Resolution Unmanned Aerial Vehicle (UAV) Imagery, Based on Structure from Motion (SfM) Point Clouds. *Remote. Sens.* **2012**, *4*, 1392–1410. https://doi.org/10.3390/rs4051392.
28. Furukawa, Y.; Ponce, J. Accurate, Dense, and Robust Multiview Stereopsis. *IEEE Trans. Pattern Anal. Mach. Intell.* **2010**, *32*, 1362–1376. https://doi.org/10.1109/tpami.2009.161.
29. Nuth, C.; Kaab, A. Co-registration and bias corrections of satellite elevation data sets for quantifying glacier thickness change. *Cryosphere* **2011**, *5*, 271–290. https://doi.org/10.5194/tc-5-271-2011.
30. Rolstad, C.; Haug, T.; Denby, B. Spatially integrated geodetic glacier mass balance and its uncertainty based on geostatistical analysis: Application to the western Svartisen ice cap, Norway. *J. Glaciol.* **2009**, *55*, 666–680. https://doi.org/10.3189/002214309789470950.
31. Huss, M.; Bauder, A.; Funk, M. Homogenization of long-term mass-balance time series. *Ann. Glaciol.* **2009**, *50*, 198–206. https://doi.org/10.3189/172756409787769627.
32. Klug, C.; Bollmann, E.; Galos, S.P.; Nicholson, L.; Prinz, R.; Rieg, L.; Sailer, R.; Stoetter, J.; Kaser, G. Geodetic reanalysis of annual glaciological mass balances (2001–2011) of Hintereisferner, Austria. *Cryosphere* **2018**, *12*, 833–849. https://doi.org/10.5194/tc-12-833-2018.
33. Ming, J.; Xiao, C.; Wang, F.; Li, Z.; Li, Y. Grey Tienshan Urumqi Glacier No.1 and light-absorbing impurities. *Environ. Sci. Pollut. Res.* **2016**, *23*, 9549–9558. https://doi.org/10.1007/s11356-016-6182-7.
34. Kraaijenbrink, P.; Meijer, S.W.; Shea, J.M.; Pellicciotti, F.; De Jong, S.M.; Immerzeel, W.W. Seasonal surface velocities of a Himalayan glacier derived by automated correlation of unmanned aerial vehicle imagery. *Ann. Glaciol.* **2016**, *57*, 103–113. https://doi.org/10.3189/2016AoG71A072.
35. Wigmore, O.; Mark, B. Monitoring tropical debris-covered glacier dynamics from high-resolution unmanned aerial vehicle photogrammetry, Cordillera Blanca, Peru. *Cryosphere* **2017**, *11*, 2463–2480. https://doi.org/10.5194/tc-11-2463-2017.
36. Liu, Y.; Qin, X.; Guo, W.; Gao, S.; Chen, J.; Wang, L.; Li, Y.; Jin, Z. Influence of the use of photogrammetric measurement precision on low-altitude micro-UAVs in the glacier region. *J. Remote Sens.* **2020**, *24*, 161–172.
37. Aoki, T.; Motoyoshi, H.; Kodama, Y.; Yasunari, T.J.; Sugiura, K.; Kobayashi, H. Atmospheric Aerosol Deposition on Snow Surfaces and Its Effect on Albedo. *Sola* **2006**, *2*, 13–16. https://doi.org/10.2151/sola.2006-004.
38. Azzoni, R.S.; Senese, A.; Zerboni, A.; Maugeri, M.; Smiraglia, C.; Diolaiuti, G.A. Estimating ice albedo from fine debris cover quantified by a semi-automatic method: The case study of Forni Glacier, Italian Alps. *Cryosphere* **2016**, *10*, 665–679. https://doi.org/10.5194/tc-10-665-2016.
39. Moeller, M.; Schneider, C.; Kilian, R. Glacier change and climate forcing in recent decades at Gran Campo Nevado, southernmost Patagonia. *Ann. Glaciol.* **2007**, *46*, 136–144. https://doi.org/10.3189/172756407782871530.
40. Fujita, K.; Ageta, Y. Effect of summer accumulation on glacier mass balance on the Tibetan Plateau revealed by mass-balance model. *J. Glaciol.* **2000**, *46*, 244–252. https://doi.org/10.3189/172756500781832945.
41. Moelg, T.; Maussion, F.; Yang, W.; Scherer, D. The footprint of Asian monsoon dynamics in the mass and energy balance of a Tibetan glacier. *Cryosphere* **2012**, *6*, 1445–1461. https://doi.org/10.5194/tc-6-1445-2012.
42. Liu, C.; Xie, Z.; Wang, C. A Research on the Mass Balance Processes of Glacier No.1 at the Headwaters of the Urumqi River, Tianshan Mountains. *J. Glaciolgy Geocryol.* **1997**, *1*, 19–26.
43. Li, D.; Liu, X.; Li, W.; Lin, Z.; Zhu, B.; Li, Z.; Li, J.; Li, B.; Fan, S.; Xie, J.; et al. Scalable and hierarchically designed polymer film as a selective thermal emitter for high-performance all-day radiative cooling. *Nat. Nanotechnol.* **2021**, *16*, 153–158. https://doi.org/10.1038/s41565-020-00800-4.
44. Nuesser, M.; Dame, J.; Krause, B.; Baghel, R.; Schmidt, S. Socio-hydrology of "artificial glaciers" in Ladakh, India: Assessing adaptive strategies in a changing cryosphere. *Reg. Environ. Change* **2019**, *19*, 1327–1337. https://doi.org/10.1007/s10113-018-1372-0.
45. Sharma, A. Giving Water Its Place: Artificial Glaciers and the Politics of Place in a High-Altitude Himalayan Village. *Water Altern.* **2019**, *12*, 993–1016.
46. Fischer, A.; Olefs, M.; Abermann, J. Glaciers, snow and ski tourism in Austria's changing climate. *Ann. Glaciol.* **2011**, *52*, 89–96. https://doi.org/10.3189/172756411797252338.
47. Li, J.; Liang, Y.; Li, W.; Xu, N.; Zhu, B.; Wu, Z.; Wang, X.; Fan, S.; Wang, M.; Zhu, J. Protecting ice from melting under sunlight via radiative cooling. *Sci. Adv.* **2022**, *8*, eabj9756. https://doi.org/10.1126/sciadv.abj9756.
48. Li, Z. *Annual Report of Tianshan Glaciological Station*; Northwest Institute of Eco-Environment and Resources, University of Chinese Academy of Sciences: Beijing, China, 2016.